JPE 18-6-1

https://doi.org/10.6113/JPE.2018.18.6.1619
ISSN(Print): 1598-2092 / ISSN(Online): 2093-4718

Double-Input DC-DC Converter for Applications with Wide-Input-Voltage-Ranges

Renjun Hu[**], Jun Zeng[**], Junfeng Liu[*], and Jinming Yang[†]

[†,**]School of Electric power, South China University of Technology, Guangzhou, China
[*]School of Automation Science and Engineering, South China University of Technology, Guangzhou, China

Abstract

The output power of most facilities for renewable energy generation is unstable due to external environmental conditions. In distributed power systems with two or more sources, a stable output can be achieved with the complementary power supply among the different input sources. In this paper, a double-input DC-DC converter with a wide-input-voltage-range is proposed for renewable energy generation. This converter has the following advantages: the circuit is simple, and the input voltage range is wide and the fault tolerance is excellent. The operation modes and the steady-state analysis are examined. Finally, experimental results are illustrated to verify the correctness of the analysis and the feasibility of the proposed converter.

Key words: Distributed power system, Double-input, Fault tolerance, Wide-input-voltage-range

I. INTRODUCTION

With the decline of the fossil fuel industry and the increase of pollution, renewable energy sources have been receiving more attention [1], [2]. These days, renewable energy sources such as solar, wind and fuel cells are being widely used. However, due to their intermittent nature, a power imbalance exists between renewable sources and the load. A distributed system with several renewable sources is proposed to solve this problem [3]. In addition, output voltages change significantly for renewable energy sources. Thus, a wide-input-voltage-range characteristic is necessary for these applications. Traditionally, several separate converters connected to a common dc bus are employed to compose a distributed power system. However, this type of configuration is relatively complex due to its multistage energy conversion and communication between converters [4]. Thus, a multiple input converter (MIC) can be a good candidate to connect several complementary renewable sources. When compared with conventional structures, systems based on a MIC have more advantages such as a simpler structure, higher power density and lower cost [5].

MICs can be classified into two categories: isolated MICs and non-isolated MICs. An isolated MIC can be constructed by multi-winding transformer and full bridge structure. It can accommodate multiple ports with different voltage levels and it can achieve electrical isolation for all of the ports. By using phase shift control, all of the switches of the converter can achieve zero voltage switching (ZVS) [6]-[9]. To accomplish a wider range of ZVS, a series resonant circuit is introduced into the full bridge structure [10]. These MICs are good candidates for applications where galvanic isolation is necessary. However, these converters need a lot of power devices due to the utilization of full bridge structures. This leads to low efficiency, low power density and a complex modulation strategy. Therefore, non-isolated MICs are appropriate for some applications where isolation is not necessary. This is due in large part to their higher efficiency, higher power density and lower cost.

Most non-isolated MICs are constituted with basic structures including buck and boost converters. By changing the combination of the basic structure, a non-isolated MIC can be generated to accommodate specific applications [11]-[13]. A three-input DC-DC boost converter is proposed in [12]. The converter is integrated with three boost units and it can connect three voltage sources simultaneously. However, the input voltages of the converter must be less than the

Manuscript received Feb. 24, 2018; accepted Jul. 1, 2018
Recommended for publication by Associate Editor Fuxin Liu.
[†]Corresponding Author: jefferliu@aliyun.com
Tel: +86-020-87110613, Fax: +86-020-87110613, South China Univ. Technol.
[*]Sch. Autom. Science Eng., South China Univ. Technol., China
[**]School of Electric power, South China Univ. Technol., China

output voltage, which limits the application of the converter. A parallel-connected MIC is proposed in [13], and this converter can work in different modes such as buck, boost and buck-boost modes. However, the input sources of the converter cannot deliver energy to the load simultaneously. Two-input buck dc-dc converters are proposed in [14]-[17], and the two sources of the converters can power loads individually or simultaneously. Inductor current ripple is analyzed in [15] and an interleaved dual-edge modulation scheme is proposed to reduce the inductor current ripple. In [16], a control method is proposed to eliminate the interaction between the control loops and to simplify the design of the controller. However, the fault tolerance of these converters is limited, and the output voltage cannot be maintained at the rating value when one input source stops powering the load. In [18], a source-port-tolerant series-connected dc-dc converter with a bootstrap circuit is proposed. The converter can solve the fault tolerance problem in some designated occasions.

In [19], a novel double-input dc-dc converter is derived from [18]. When compared to [18], the derived converter saves a bootstrap capacitor, which results in a peak current during the charging process. Based on the structure in [19], the detailed analysis and experimental waveforms are given in this paper. As a result, the wide input voltage range characteristic and fault tolerant ability of the converter are demonstrated.

II. The Operation Principles

The converter in [18] is shown in Fig. 1. The diode D_{C1} and the switch S_{C1} are key components in the derivation process. As shown in Fig. 2, D_{C1} and S_{C1} are moved to a location between the inductor L and the output capacitor C_o. Since the bootstrap capacitor is useless, C_o and D_{in1} can be removed from the converter.

As shown in Fig. 3, the proposed converter can be obtained by rearranging the derivation circuit. V_{in1} and V_{in2} are the voltages of the input sources, S_1, S_2 and S_3 are switches, D_1 and D_2 are freewheeling diodes, L is the filter inductor, C_o is the output capacitor, R is the load, and V_o is the output voltage.

According to the input voltages of the input sources, the converter can work in three modes. When the voltages are large enough, the converter works in mode I, where the output voltage is smaller than the sum of the input voltages. When the input voltages decrease gradually, the converter transfers to mode II, where output voltage may be larger or smaller than the sum of the input voltages. If one of the input sources quits, the converter works in the fault-tolerant mode.

A. The Operation Principles of Mode I

In this mode, S_3 is kept OFF, and there are three switching states in one operating period. The key waveforms of this mode are shown in Fig. 4(a), where G_{S1} and G_{S2} are the driving signals for S_1 and S_2 with duty cycles of D_{S1} and D_{S2},

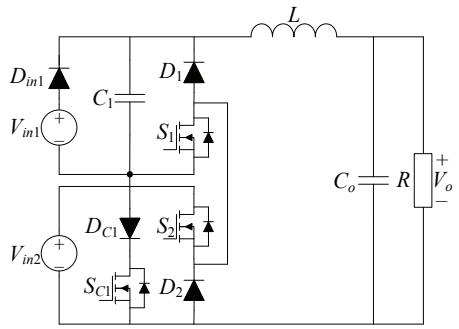

Fig. 1. Circuit of the converter proposed in [18].

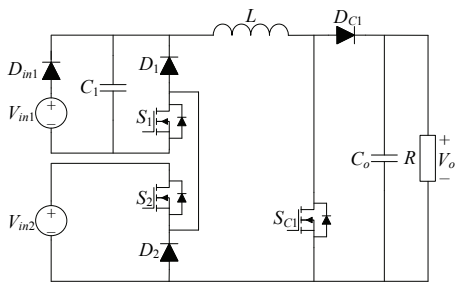

Fig. 2. Derivation process of the proposed converter.

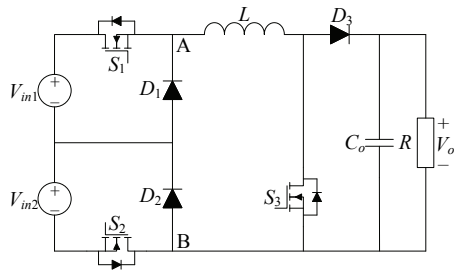

Fig. 3. Circuit of the proposed converter.

respectively. T_S is the switch period, V_{AB} is the voltage between points A and B, and i_L is the current flowing through the inductor L. Equivalent circuits for each of the states are given in Fig. 5.

State I [see Fig. 5(a)]: S_1 is ON and S_2 is OFF. V_{AB} is V_{in1}, the load absorbs energy from V_{in1}, and i_L increases linearly when $V_{in1}>V_o$ and decreases linearly when $V_{in1}<V_o$.

$$L\frac{d_{i_L}}{d_t} = V_{in1} - V_o \tag{1}$$

State II [see Fig. 5(b)]: S_1 and S_2 are both OFF. V_{AB} is zero, L supplies energy to the load, and i_L decreases linearly.

$$L\frac{d_{i_L}}{d_t} = -V_o \tag{2}$$

State III [see Fig. 5(d)]: S_1 is OFF and S_2 is ON. V_{AB} is V_{in2}, the load absorbs energy from V_{in2}, and i_L increases linearly when $V_{in2}>V_o$ and decreases linearly when $V_{in2}<V_o$.

$$L\frac{d_{i_L}}{d_t} = V_{in2} - V_o \tag{3}$$

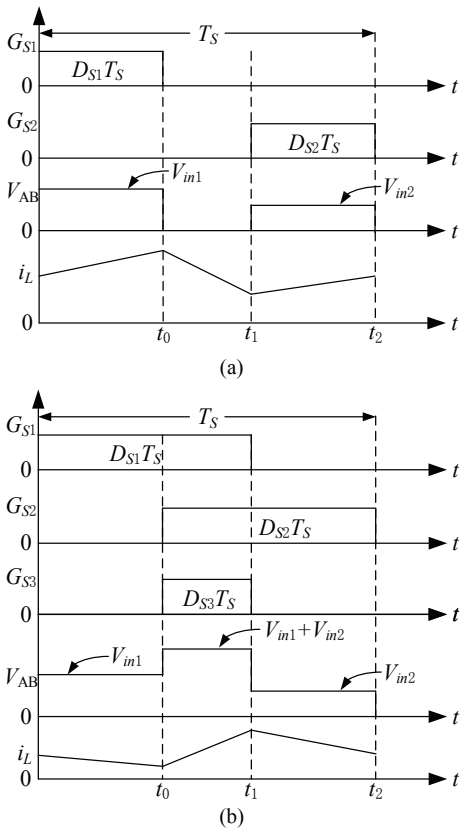

Fig. 4. Key waveforms of the converter: (a) Mode I; (b) Mode II.

B. The Operation Principles of Mode II

In this mode, S_3 takes part in the power transmission, and there are three switching states in one operating period. In this section, state II will be introduced alone. This is due to the fact that the switching states in this mode are same as those in mode I with the exception of state II. Key waveforms are shown in Fig. 4(b), where G_{S3} is the driving signal for S_3 with a duty cycle of D_{S3}. The equivalent circuit of state II is given in Fig. 5.

State II [see Fig. 5(c)]: S_1, S_2 and S_3 are ON. V_{AB} is the sum of V_{in1} and V_{in2}, L absorbs energy from two input sources, and i_L increases linearly.

$$L\frac{d_{i_L}}{d_t} = V_{in1} + V_{in2} \tag{4}$$

C. The Operation Principles of the Fault-Tolerant Mode

In this mode, only one input source supplies energy to the load. Due to the symmetry of the proposed converter, it is enough to introduce the situation where V_{in1} supplies energy to the load alone.

The proposed converter can work as a conventional buck or boost converter. The buck converter has two switching states in one operating period, and equivalent circuits are shown in Fig. 5(a) and (b). Similarly, the boost converter also has two switching states in one operating period, and equivalent circuits are shown in Fig. 5(a) and (e).

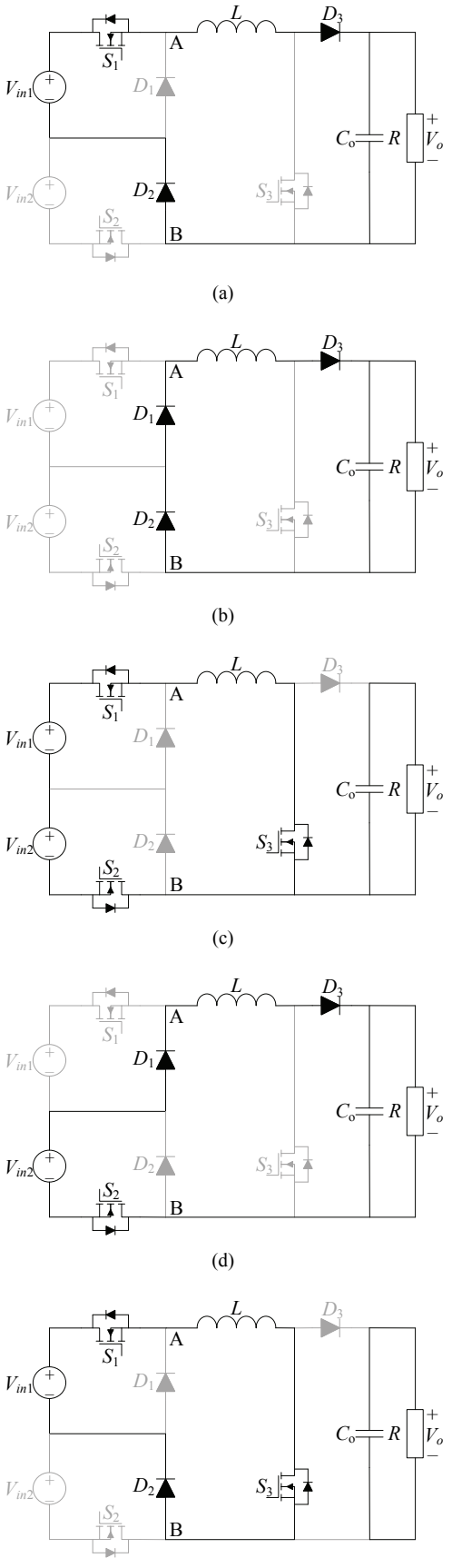

Fig. 5. Equivalent circuits of the switching states.

III. The Steady-State Analysis

A. The Analysis of Voltage Gain

Before the analysis, it is assumed that all of the devices of the converter are ideal and that the inductor current is continuous.

In mode I, applying the voltage-second balance to L, the following equation can be obtained:

$$V_0(1-D_{S1}-D_{S2})=(V_{in1}-V_o)D_{S1}+(V_{in2}-V_0)D_{S2} \quad (5)$$

Thus, V_o can be derived as:

$$V_o=V_{in1}D_{S1}+V_{in2}D_{S2} \quad (6)$$

In mode II, applying the voltage-second balance to L, the following equation can be obtained:

$$(V_{in1}+V_{in2})D_{S3}=(V_0-V_{in1})D_{S1}+(V_0-V_{in2})D_{S2} \quad (7)$$

V_o can be derived as:

$$V_o=\frac{V_{in1}D_{S1}+V_{in2}D_{S2}}{1-D_{S3}} \quad (8)$$

From Fig. 4(b), it can be found that:

$$D_{S3}=D_{S1}+D_{S2}-1 \quad (9)$$

By substituting (9) into (8), equation (8) can be rewritten as:

$$V_o=\frac{V_{in1}D_{S1}+V_{in2}D_{S2}}{2-D_{S1}-D_{S2}} \quad (10)$$

For the fault-tolerant mode, the proposed converter is a buck converter when $V_{in1}>V_o$. The relationship between V_{in1} and V_o can be derived as:

$$V_o=V_{in}D_{S1} \quad (11)$$

The proposed converter is a boost converter when $V_{in1}<V_o$. The relationship between V_{in1} and V_o can be derived as:

$$V_o=\frac{V_{in}}{1-D_{S1}} \quad (12)$$

B. The Wide-Input-Voltage-Range Characteristic

The equations of (6) and (10) have given the input-output relationship of the proposed converter. It can be found that the output voltage is determined by V_{in1}, V_{in2}, D_{S1} and D_{S2} in both modes I and II. To observe the input voltage range intuitionally, the relationship curves of V_{in2} and D_{S2} are demonstrated in Fig. 6 with fixed values of V_{in1}, D_{S1} and V_o.

In Fig. 6(a), V_{in1} is 30 V and V_o is 50 V. The three curves can be plotted when D_{S1} is 0.4, 0.5 and 0.6. When S_3 is kept OFF, the relationship curves between V_{in2} and D_2 are A_0A_2, B_0B_2 and C_0C_2, respectively. When the converter adopts the proposed modulation scheme, the relationship curves are A_0A_3, B_0B_3 and C_0C_3. A_1, B_1 and C_1 are critical points between modes I and II.

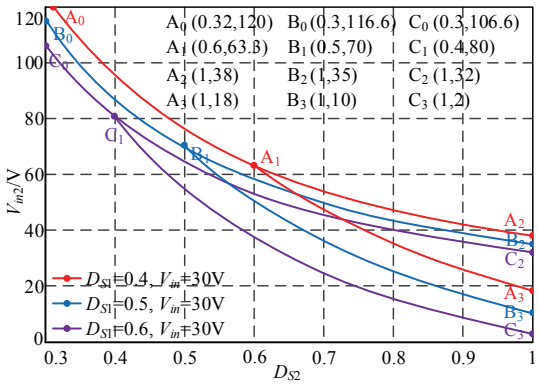

(a)

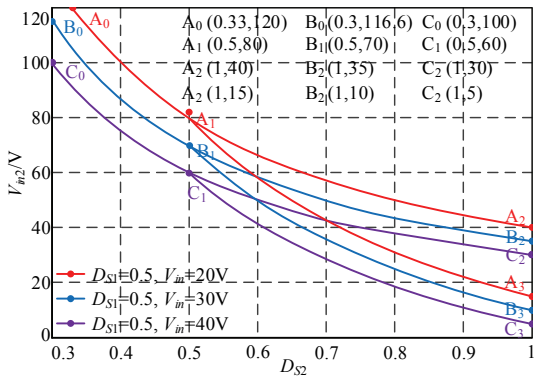

(b)

Fig. 6. The relationship curves of V_{in2} and D_{S2}: (a) V_{in1}=30 V, D_1=0.4, 0.5 or 0.6; (b) D_1=0.5, V_{in1}=30 V, 40 V or 50 V.

In Fig. 6(b), D_{S1} is 0.5, and V_o is 50 V. Three curves can be plotted when V_{in1} is 20 V, 30 V and 40 V. When S_3 is kept OFF, the relationship curves between V_{in2} and D_2 are A_0A_2, B_0B_2 and C_0C_2, respectively. When the converter adopts the proposed modulation scheme, the relationship curves are A_0A_3, B_0B_3 and C_0C_3. A_1, B_1 and C_1 are critical points between modes I and II.

According to Fig. 6, it is obvious that the input voltage range becomes wider under the proposed modulation scheme. Hence, the wide-input-voltage-range characteristic is achieved.

C. The Fault-Tolerant Capability

A double-input converter is proposed for renewable energy generation systems, and the input sources may stop powering the load due to their intermittent nature. Thus, it is necessary to discuss the fault-tolerant capability of the converter. A schematic diagram of the fault-tolerant capability is shown in Fig. 7.

When V_{in2} is 0, the converter has three working states with different values of V_{in1}. When $0.2V_o<V_{in1}<V_o$, the proposed converter operates as a boost converter. When $V_o<V_{in1}<5V_o$, the proposed converter operates as a buck converter. When $V_{in1}<0.2V_o$ and $V_{in1}>5V_o$, the converter breaks down due to limitations of the voltage gain. Similarly, when V_{in1} is 0, the converter has three working states with different values of

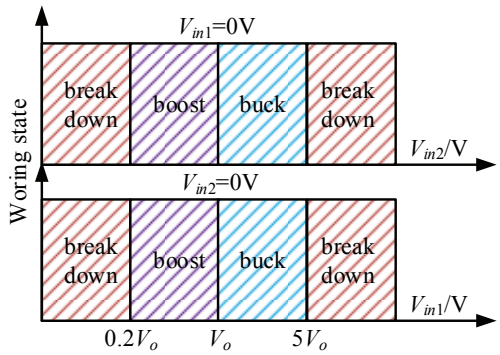

Fig. 7. Schematic diagram of the fault-tolerant capability.

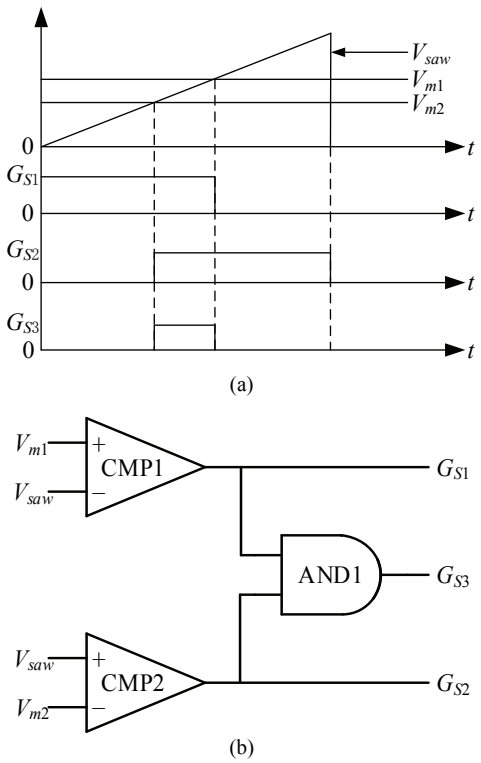

Fig. 8. Modulation scheme and logic circuit: (a) Modulation scheme; (b) Logic circuit.

V_{in2}. The working states are the same as the situation described above. Consequently, the proposed converter has excellent fault-tolerant capability when two input sources vary from 0.2V_o to 5V_o.

IV. Modulation Scheme

Fig. 8(a) shows the modulation scheme of the proposed converter, where V_{saw} is the saw-tooth carrier, and the dc variables V_{m1} and V_{m2} are the modulation signals. G_{S1} and G_{S2} are obtained by comparing the saw-tooth carrier and the modulation signals. When V_{m1} is larger than V_{saw}, G_{S1} is generated. Similarly, G_{S2} is obtained when V_{saw} is larger than V_{m2}. G_{S3} can be derived by the logical operation of the signals G_{S1} and G_{S2}:

TABLE I
Parameters of the Proposed Converter

Comparison items	Proposed converter	[16]	[18]
Switch number	3	2	3
Diode number	3	2	4
Minimum input voltage	10 V	35 V	35 V
Fault-tolerant ability	(0.2V_o,5V_o)	(V_o,5V_o)	(V_o,5V_o)
	(0.2V_o,5V_o)	(0.5V_o,5V_o)	(V_o,5V_o)
Efficiency	94.16%	95.51%	95.35%

$$G_{S3} = G_{S1} \bullet G_{S2} \tag{13}$$

Fig. 8(b) shows a logical circuit of the modulation scheme, where CMP1 and CMP2 are comparators, and AND1 is the AND gate. G_{S1} and G_{S2} are generated by CMP1 and CMP2, respectively. G_{S3} is generated by AND1.

In this modulation scheme, all of the switches are controlled by two modulation signals that are determined by the voltages of two input sources. The logic circuit is simple and only needs three logic gates. The converter can transfer between modes I and II with a change of the input voltages.

V. Comparisons with Existing Converters

Comparisons are conducted among the proposed converter and the converters in [16] and [18]. These comparisons include components number, minimum input voltage, fault-tolerant capability and theoretical efficiency.

As shown in Table I, the proposed converter needs more components when compared with the converter in [16]. Meanwhile, the performance of the proposed converter has been significantly improved. When V_{in1} is 30 V and D_{S1} is 0.5, the minimum voltage of V_{in2} is 10 V, which is a lot less than the 35 V minimum voltage of the converters in [16] and [18]. On the other hand, the maximum voltages of the three converters are the same. Thus, the proposed converter has a wider input voltage range. In terms of system reliability, the proposed converter can achieve fault-tolerance with a full input voltage range when V_{in1} and V_{in2} vary from 0.2V_o to 5V_o. The tolerant input voltage ranges of the three converters are listed, and the proposed converter obviously has an advantage when compared with the other two converters. Finally, the theoretical efficiencies are compared when the three converters operate at 100 W with the same parameters. It can be seen that the proposed converter sacrifices some of its efficiency to improve the system performance.

VI. Experimental Verifications

To validate the performance of the proposed converter, a 100W prototype was built, and extensive experiments were carried out. As shown in Fig. 9, the converter is controlled by

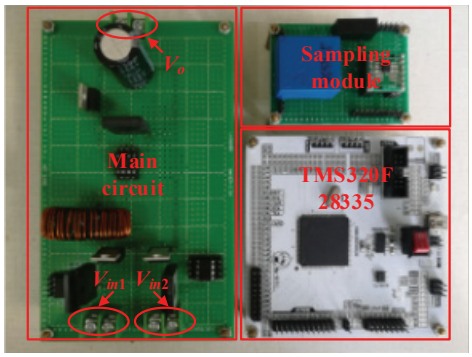

Fig. 9. Experimental prototype.

TABLE II
PARAMETERS OF THE PROPOSED CONVERTER

Parameter	Value
Output voltage (V_o)	50 V
Rating power (P_o)	100 W
Output capacitor (C_o)	220 μF
Inductor (L)	300 μH
Switching frequency (f_s)	30 kHz

TABLE III
TYPES OF INSTRUMENTS AND COMPONENTS

Type	Name	Model
Instrument	Controller	TMS320F28335
	Power supply	QJ-3005S III (V_{in1}) JP10020D (V_{in2})
	Oscilloscope	RIGOL DS4014E
Component	Switches (S_1-S_3)	IRFP250
	Diodes (D_1-D_3)	SR5200
	Capacitor (C_o)	Electrolytic capacitor

a digital signal processor TMS320F28335 that generates three driving signals for S_1-S_3. The main parameters of the converter are shown in Table II. The types of instruments and components used in the experiments are shown in Table III.

A. Steady-State Experiment

Key steady-state waveforms are shown in Fig. 10, Fig. 11, and Fig. 12. Fig. 10 shows experimental waveforms of mode I, in which V_{in1} is 30 V and V_{in2} is 80 V. As shown in Fig. 10(a), S_3 is kept OFF all the time, and V_o is 50 V. Fig. 10(b) shows waveforms of the inductor current i_L. When S_1 turns ON, the voltage over the inductor is V_{in1}-V_o, and i_L decreases linearly. When S_1 turns OFF, the voltage over the inductor is -V_o, i_L keeps decreasing, and the descent rate is larger than that in first state. When S_2 turns ON, the voltage over the inductor is V_{in2}, and i_L begins to increases linearly.

Fig. 11 shows experimental waveforms of mode II, in which V_{in1} is 30 V and V_{in2} is 15 V. As shown in Fig. 11(a), G_{S3} is generated by G_{S1} and G_{S2}, and V_o is 50 V. Fig. 11(b) shows waveforms of the inductor current i_L. When S_1 turns

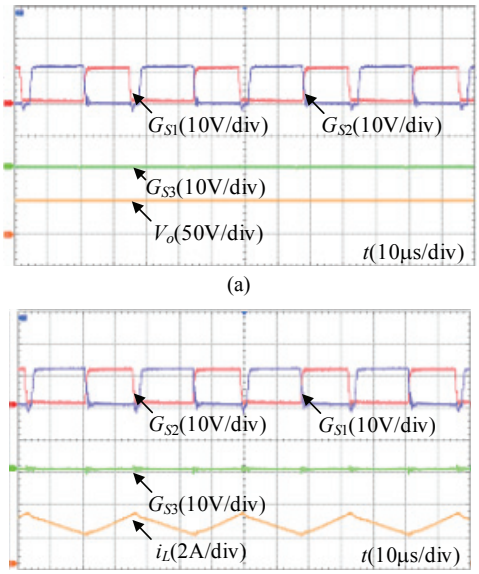

Fig. 10. Experimental waveforms of mode I (V_{in1}=30 V, V_{in2}=80 V): (a) Waveform of the output voltage; (b) Waveform of the inductor current.

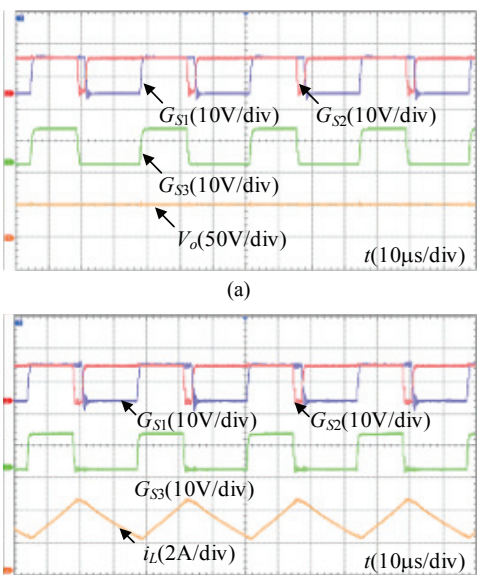

Fig. 11. Experimental waveforms of mode II (V_{in1}=30 V, V_{in2}=15 V): (a) Waveform of the output voltage; (b) Waveform of the inductor current.

ON, the voltage over the inductor is V_{in1}- V_o, and i_L decreases linearly. When S_1 and S_2 turn ON, the voltage over the inductor is V_{in1}+V_{in2}, and i_L increases rapidly. When S_1 turns OFF, the voltage over the inductor is V_{in2}-V_o, i_L decreases linearly, and the descent rate is smaller than that in first state.

Fig. 12 shows experimental waveforms of the fault tolerant mode. In this mode, only V_{in1} supplies energy to the load, and the converter works as a boost or buck converter. In Fig. 12(a), V_{in1} is 30 V, S_1 is kept ON all the time, and the converter works as a boost converter. When S_3 turns ON, the

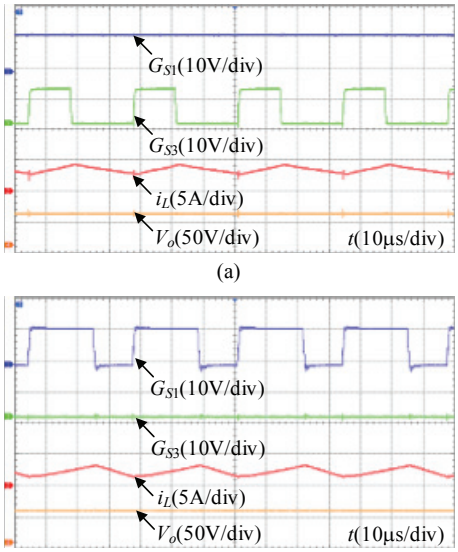

Fig. 12. Experimental waveforms of the fault-tolerant mode (V_{in2}=0 V): (a) Waveforms of a boost converter (V_{in1}=30 V); (b) Waveforms of a buck converter (V_{in1}=80 V).

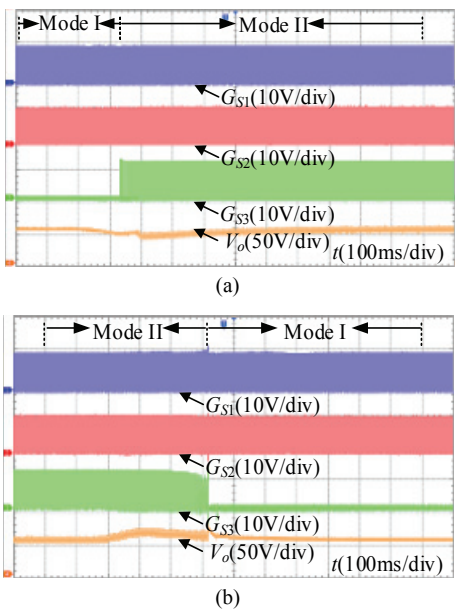

Fig. 13. Experimental waveforms of mode transitions: (a) Mode I to mode II; (b) Mode II to mode I.

voltage over the inductor is V_{in1}, and i_L increases linearly. When S_3 turns OFF, the voltage over the inductor is V_{in1}-V_o, and i_L decreases linearly. In Fig. 12(b), V_{in1} is 80 V, S_3 is kept OFF all the time, and the converter works as a buck converter. When S_1 turns ON, the voltage over the inductor is V_{in}-V_o, and i_L increases linearly. When S_1 turns OFF, the voltage over the inductor is -V_o, and i_L decreases linearly. These experimental results verify the theoretical analysis.

B. Mode Transition Experiment

Transient waveforms with stepping up and down V_{in2} are demonstrated in Fig. 13. In Fig. 13(a), it can be found that the converter is shifted from mode I to mode II when V_{in2} is stepped down from 80 V to 30 V. After the stepping down of V_{in2}, V_o goes down, and then it goes up until stabilizing at 50 V. In Fig. 13(b), the converter is shifted from mode II to mode I when V_{in2} is stepped up from 30 V to 80 V. After the stepping up of V_{in1}, V_o goes up, and then it goes down until stabilizing at 50 V. The experiment results show that the converter can shift freely between mode I and mode II.

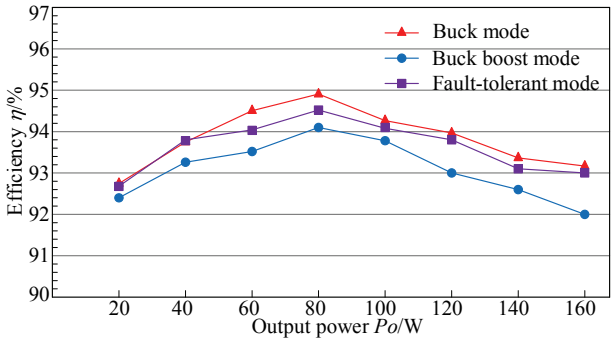

Fig. 14. Efficiency in different operation modes.

C. Efficiency Analysis

Efficiency curves of the converter are shown in Fig. 14. The efficiency of the converter is about 92%-95% when the output power P_o is in the range of 20 W-160 W. It can be found that the efficiency of mode I is higher than that of mode II. Mode III has the highest efficiency among the three modes.

VII. Conclusions

A double-input dc-dc converter is proposed for wide-input-voltage-range applications in this paper. It is suitable for distributed power systems with two renewable energy sources such as wind-photovoltaic complementary power generation systems. The converter has two input ports, and the input sources can deliver energy to the load individually or simultaneously. Since the converter can work in two modes, a wide input range is feasible. A modulation strategy is introduced that allows the converter to smoothly transfer from mode I to mode II. Furthermore, if one of the input sources is powered off, the converter can work as a boost or buck circuit to maintain a stable output voltage. The experimental results verify the correctness of the analysis and the feasibility of the proposed converter.

Acknowledgment

The authors gratefully acknowledge the financial support the financial support of National Natural Science Foundation of China (No. 61573155& 51877085), Guangdong Natural Science Foundation (No.2016A030313508), Guangdong Science and Technology Planning (No.2016A010102007).

REFERENCES

[1] A. I. Bratcu, I. Munteanu, S. Bacha, D. Picault, and B. Raison, "Cascaded DC–DC converter photovoltaic systems: Power optimization issues," *IEEE Trans. Ind. Electron.*, Vol. 58, No. 2, pp. 403-411, Feb. 2011.

[2] M. Cacciato, A. Consoli, R. Attanasio, and F. Gennaro. "Soft-switching converter with HF transformer for grid-connected photovoltaic systems," *IEEE Trans. Ind. Electron.*, Vol. 57, No. 5, pp. 1678-1688, Sep. 2009.

[3] L. J. Chien, C. C. Chen, J. F. Chen, and Y. P. Hsieh, "Novel three-port converter with high-voltage gain," *IEEE Trans. Power Electron.*, Vol. 29, No. 9, pp. 4693-4703, Oct. 2013.

[4] K. Jin, X. Ruan, M. Yang, and M. Xu, "A hybrid fuel cell power system," *IEEE Trans. Ind. Electron.*, Vol. 56, No. 4, pp. 1212-1222, Apr. 2009.

[5] Y. M. Chen, Y. C. Liu, and S. H. Lin, "Double-input PWM DC/DC converter for high-/low-voltage sources," *IEEE Trans. Ind. Electron.*, Vol. 53, No. 5, pp. 1538-1545, Oct. 2006.

[6] Y. M. Chen, Y. C. Liu, and F. Y. Wu, "Multi-input DC/DC converter based on the multi-winding transformer for renewable energy applications," *IEEE Trans. Ind. Appl.*, Vol.38, No.4, pp. 1096-1104, Aug. 2002.

[7] J. L. Duarte, M. Hendrix, and M. G. Simoes, "Three-port bidirectional converter for hybrid fuel cell systems," *IEEE Trans. Power Electron.*, Vol. 22, No. 2, pp. 480-487, Mar. 2007.

[8] C. Zhao, S. D. Round, and J. W. Kolar, "An isolated three-port bidirectional DC-DC converter with decoupled power flow management," *IEEE Trans. Power Electron.*, Vol. 23 No. 5, pp. 2443-2453, Nov. 2008.

[9] H. Tao, J. L. Duarte, and M. A. M. Hendrix, "Three-port triple-half-bridge bidirectional converter with zero-voltage switching," *IEEE Trans. Power Electron.*, Vol. 23, No. 2, pp. 782-792, Mar. 2008.

[10] H. Krishnaswami and N. Mohan, "Three-port series-resonant dc–dc converter to interface renewable energy sources with bidirectional load and energy storage ports," *IEEE Trans. Power Electron*., Vol. 24, No. 10, pp. 2289-2297, Aug. 2009.

[11] Y. C. Liu and Y. M. Chen, "A systematic approach to synthesizing multi-input DC–DC converters," *IEEE Trans. Power Electron.*, Vol. 24, No. 1, pp. 116-127, Feb. 2009.

[12] F. Nejabatkhah, S. Danyali, S. H. Hosseini, and M. Sabahi, "Modeling and control of a new three-input DC–DC boost converter for hybrid PV/FC/Battery power system," *IEEE Trans. Power Electron.*, Vol. 27, No. 5, pp. 2309-2324, Oct. 2011.

[13] A. Khaligh, J. Cao, and Y. J. Lee, "A multiple-input DC–DC converter topology," *IEEE Trans. Power Electron.*, Vol. 24, No. 3, pp. 862-868, Mar. 2009.

[14] Y. Li, X. Yuan, and D. Yang, "A new double-input DC-DC converter," *Trans. China Electrotech. Soc.*, Vol. 23, No. 6, pp. 121-125, Jun. 2008.

[15] Y. Li, X. Yuan, and D. Yang, "Interleaved dual-edge modulation scheme for double-input buck converter," *Trans. China Electrotech. Soc.*, Vol. 24, No. 4, pp. 139-146, Apr. 2009.

[16] D. Yang, M. Yang, and X. Ruan, "One-cycle control for a double-input DC/DC converter," *IEEE Trans. Power Electron.*, Vol. 27, No. 11, pp. 4646-4655, Nov. 2012.

[17] Y. Li, X. Yuan, D. Yang, and F. Liu, "Modeling and design of control system for double-input DC/DC converter," *Trans. China Electrotech. Soc.* Vol. 25, No. 11, pp. 47-54, Nov. 2010.

[18] X. Sun, Y. Zhou, W. Wang, B. Wang, and Z. Zhang, "Alternative source-port-tolerant series-connected double-input DC–DC converter," *IEEE Trans. Power Electron.*, Vol. 30, No. 5, pp. 2733-2742, May 2015.

[19] R. Hu, J. Zeng, and J. Liu, "A double-input DC-DC converter for wide-input-voltage-range application," in *Proc. PESA*, pp. 1-5, 2017.

Renjun Hu was born in Hubei, China, in 1993. He received his B.S. degree in Process Automation from the Wuhan Institute of Technology, Wuhan, China, in 2015. He is presently working towards his M.S. and Ph.D. degrees in Power Electronics and Motor Drives at the South China University of Technology, Guangzhou, China. His current research interests include DC-DC converters and multi-port converters

Jun Zeng received her Ph.D. degree in Control Theory and Control Engineering from the South China University of Technology, Guangzhou, China, in 2007. She is presently working as a Professor in the College of Electric Power, South China University of Technology, Guangzhou, China. Her current research interests include power electronic applications, energy management, intelligent control in distributed generation and the integration of renewable energy to smartgrids.

Junfeng Liu received his M.S. degree in Control Engineering from the South China University of Technology, Guangzhou, China, in 2005; and his Ph.D. degree from the Hong Kong Polytechnic University, Kowloon, Hong Kong SAR, China, in 2013. From 2005 to 2008, he was working as a Development Engineer at Guangdong Nortel Network, Guangzhou, China. In 2014, he joined the South China University of Technology, where he is presently working as an Associated Professor in the School of Automation Science and Engineering. His current research interests include power electronic applications, nonlinear control, high frequency power distribution systems and motion control systems.

Jinming Yang received his B.S. degree from the Beijing University of Aeronautics and Astronautics, Beijing, China, in 1987; his M.S. degree from Zhejiang University, Hangzhou, China, in 1990; and his Ph.D. degree from the South China University of Technology, Guangzhou, China, in 2000. From 1983 to 1987, he was a Design Engineer at the Airplane Design Institute, Guizhou, China. From 1990 to 1997, he was a Lecturer at Guizhou University, Guiyang, China. He is presently working as a Professor at the South China University of Technology. His current research interests include power conversion, microgrids, renewable energy generation technology and nonlinear control.